Oxidation of dry methane on the surface of oxygen ion-conducting membranes

A.A. Yaremchenko[a], A.A. Valente[b], V.V. Kharton[a,c,*], E.V. Tsipis[a], J.R. Frade[a], E.N. Naumovich[a,c], J. Rocha[b], and F.M.B. Marques[a]

[a]*Department of Ceramics and Glass Engineering, CICECO, University of Aveiro, 3810-193 Aveiro, Portugal*
[b]*Department of Chemistry, CICECO, University of Aveiro, 3810-193 Aveiro, Portugal*
[c]*Institute of Physicochemical Problems, Belarus State University, 14 Leningradskaya Str., 220050 Minsk, Belarus*

Received 14 August 2003; accepted 18 September 2003

The surface exchange limitations of oxygen permeation through dense mixed-conducting membranes enhance membrane stability, enabling the operation of mixed conductors, such as $La_{0.3}Sr_{0.7}Co_{0.8}Ga_{0.2}O_{3-\delta}$ (LSCG) and $La_2Ni_{0.9}Co_{0.1}O_{4+\delta}$ (LNC), under air/dry CH_4 gradient up to temperatures as high as 1173–1223 K. Testing of these materials in a model disk-shaped membrane reactor at 1023–1223 K showed high CO_2 yields (>75%). In particular, at 1173 K, the CO selectivity was 17% for LNC and 2% for LSCG ceramics, with methane conversion efficiency of 20 and 37% respectively. Similar tendency was observed for a fuel cell-type reactor with yttria-stabilized zirconia solid electrolyte and cermet $Ce_{0.8}Gd_{0.2}O_{2-\delta}$/Pt anode, where decreasing the molar ratio between methane and electrochemically supplied oxygen from approximately 10 to 2 decreases CO/CO_2 ratio at the outlet down to 0.3. This behavior suggests significant role of the complete methane oxidation on the interface between an oxygen ion-conducting membrane and gas phase, thus making it necessary to incorporate reforming catalysts in the reactors.

KEY WORDS: partial oxidation; synthesis gas; membrane; mixed conductor; solid electrolyte; perovskite; oxygen permeation; fuel cell.

1. Introduction

Synthesis gas (syngas), a mixture of carbon monoxide and hydrogen, is the most important feedstock for commercial Fischer–Tropsch and methanol synthesis [1,2]. The industrial production of synthesis gas is based on steam reforming of methane, the main component of natural gas. This process is, however, energy intensive due to the highly endothermic nature of the reaction ($CH_4 + H_2O = CO + 3H_2$, $\Delta H^0_{298} = 206\,kJ/mol$) and yields H_2/CO molar ratio higher than optimum required for further syngas conversion into hydrocarbons or methanol. One alternative route relates to the catalytic partial oxidation of methane, which is mildly exothermic ($CH_4 + 1/2O_2 = CO + 2H_2$, $\Delta H^0_{298} = -36\,kJ/mol$) and gives an optimum H_2/CO ratio of 2 [1,2]. The main cost of syngas production by the partial oxidation is associated with cryogenic oxygen plants [1–3].

Contrary to conventional technologies, the use of solid oxide fuel cells (SOFCs) and/or dense mixed-conducting membranes makes it possible to combine oxygen separation, partial oxidation and reforming of methane in a single reactor [3–11]. The development of economically feasible SOFCs is also of great interest for power generation due to high energy-conversion efficiency, fuel flexibility and environmental impact [12,13]. The use of SOFC-type reactors for the natural gas conversion requires relatively high currents and low electrode polarization; this is only possible when using catalytically active anode components such as CeO_2, which promote oxidation reactions, suppress carbon deposition and enlarge electrochemical reaction zone [14–18]. The reactors with mixed-conducting membranes can operate without external circuitry and are thus simpler compared to SOFCs. During the last decade, significant attention has been focused on perovskite-type mixed conductors $(La,A)(Co,Fe)O_{3-\delta}$ (A = Sr or Ba), tested for partial oxidation and oxidative coupling of methane [6–11]. One should mention that thermodynamic stability of cobaltite- and ferrite-based perovskites in highly reducing environments is rather insufficient [19]; the stable operation is only possible in the presence of steady state oxygen permeation flux across the membrane. As shown below, such a kinetic stabilization is achieved when the overall oxygen transport is limited by exchange rate on the membrane permeate-side surface.

The present work is focused on the evaluation of mixed-conducting $La_{0.3}Sr_{0.7}Co_{0.8}Ga_{0.2}O_{3-\delta}$ (LSCG) and $La_2Ni_{0.9}Co_{0.1}O_{4+\delta}$ (LNC) ceramics in a model reactor for direct oxidation of dry CH_4. $La_2Ni_{0.9}Co_{0.1}O_{4+\delta}$ with a K_2NiF_4-type structure and perovskite-like $La_{0.3}Sr_{0.7}CoO_{3-\delta}$ are known to exhibit substantially high oxygen permeability [20,21]. In order to suppress chemical expansion induced by the oxygen chemical

* To whom correspondence should be addressed.
E-mail: kharton@cv.ua.pt

1011-372X/03/1200–0169/0

potential variations, the perovskite phase is doped with gallium [22]. The performance of the mixed-conducting membranes is compared with that of a SOFC-type reactor made of yttria-stabilized zirconia (YSZ) electrolyte with cermet $Ce_{0.8}Gd_{0.2}O_{2-\delta}$/Pt anodes.

2. Experimental

Powders of LNC and LSCG were prepared by the glycine-nitrate process (GNP), a self-combustion synthesis technique using glycine as a fuel and nitrates of metal components as an oxidant [23]. In the course of GNP, glycine was added into aqueous nitrate solution containing metal cations in stoichiometric proportions (molar glycine/nitrate ratio of 2 : 1). After drying and firing, the resultant powders were ball-milled and annealed in air at 1073 K for 2 h. Dense ceramic samples were pressed at 300–400 MPa and then sintered in air at 1533–1553 K for 2 h. The X-ray diffraction (XRD) analysis of ceramics showed formation of single phases, with tetragonal K_2NiF_4-type structure for LNC and cubic perovskite for LSCG, in agreement with [20,21]. The density of the ceramics was 96–97% of their theoretical density calculated from XRD data.

Characterization of ceramic materials included XRD, scanning and transmission electron microscopy (SEM and TEM) coupled with energy dispersive spectroscopy (EDS), measurements of total conductivity and Seebeck coefficient as function of temperature and oxygen partial pressure, and determination of steady state oxygen permeation fluxes. A detailed description of the experimental procedures and equipment used for characterization was published elsewhere ([20–22,24] and references therein). The phase stability boundaries at reduced $p(O_2)$ were estimated from results on the total conductivity (σ) and Seebeck coefficient (α). As an example, figure 1 illustrates the determination of stability limits from the data on total conductivity at 973 K. The oxygen pressure, at which the slope of $\log\sigma$-$\log p(O_2)$ and α-$\log p(O_2)$ dependencies started to change, was considered as a stability boundary at a given temperature. Further reduction of oxygen partial pressure resulted in drastic irreversible degradation in electric properties due to phase decomposition of ceramics.

The experimental setup for the methane oxidation studies comprised a dense disk-shaped membrane,

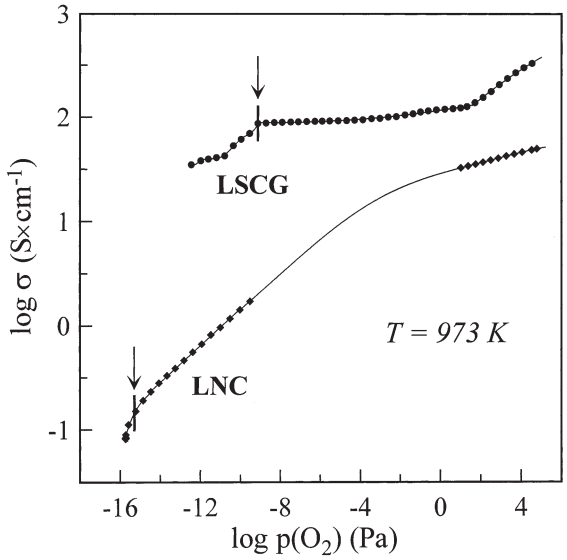

Figure 1. Oxygen partial pressure dependencies of total conductivity, illustrating the determination of phase stability limits (indicated by arrows) of LNC and LSCG.

hermetically sealed onto YSZ tube, and an electrochemical oxygen sensor at the outlet of the cell. In all cases, effective geometric area of the membrane surface exposed to methane flow was 0.64 cm^2. For LNC and LSCG membranes, catalytically active porous layers were applied onto the permeate-side surface; their composition and fabrication conditions are listed in table 1. The SOFC-type cell consisted of one YSZ disc with $Ce_{0.8}Gd_{0.2}O_{2-\delta}$/Pt cermet anode (50 : 50 wt%) and porous platinum cathode; platinum wires were used as current collectors. Nanocrystalline powder of $Ce_{0.8}Gd_{0.2}O_{2-\delta}$ (CGO) used for the anode was prepared by the cellulose-precursor technique described elsewhere [16,24]; after anode fabrication at 1273 K (table 1), the size of CGO particles determined by TEM was 20–60 nm. The anode microstructure represents a matrix of large platinum particles (0.2–2 μm), covered with porous agglomerates of nanocrystalline CGO (figure 2(a)).

In the course of steady state electrocatalytic experiments, dry CH_4 ($\geq$99.995% purity) diluted with helium was supplied onto the permeate side of a mixed-conducting membrane or onto the anode of the SOFC-type reactor, with the feed side or cathode being exposed to atmospheric air. The gas-flow composition and rate at the reactor inlet were fixed by Bronkhorst mass-flow

Table 1
Composition of porous surface layers and their preparation conditions

Membrane	Thickness d (mm)	Layer	Composition	Annealing	Sheet density (mg/cm^2)
LNC	0.60	Permeate-side surface	LNC/Pt (50 : 50 wt.%)	1273 K/h	5.6±0.1
LSCG	0.95	Permeate-side surface	Pt	1223 K/0.5 h	8.6±0.1
YSZ	0.90	Anode	CGO/Pt (50 : 50 wt.%)	1273 K/h	9±1

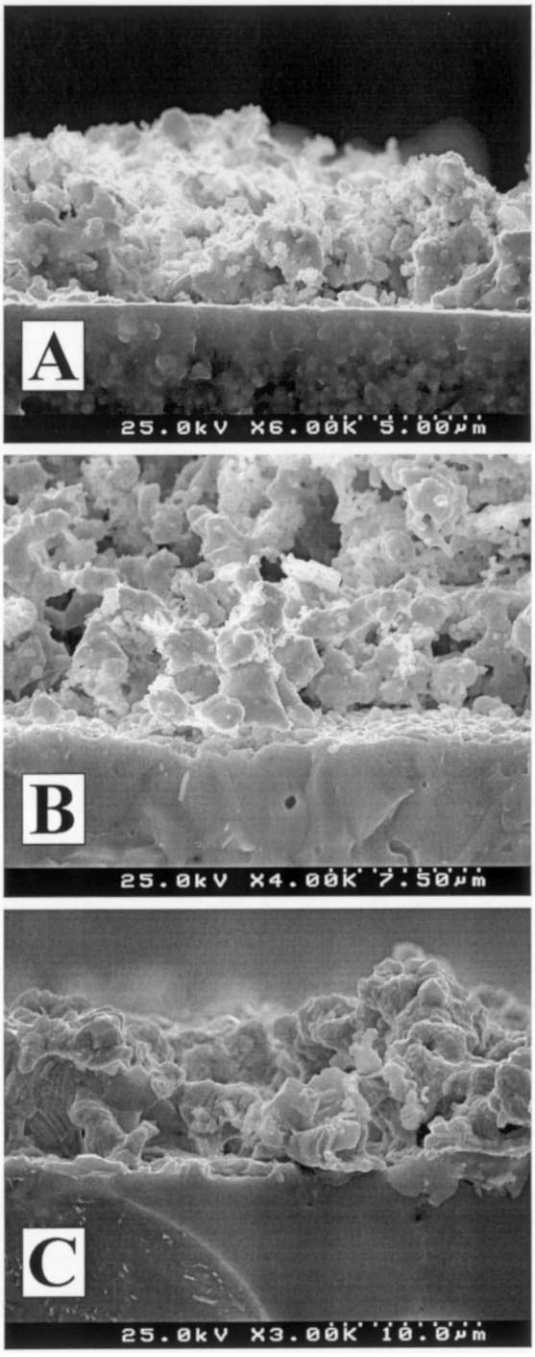

Figure 2. SEM micrographs: (A) as-prepared CGO/Pt anode on YSZ membrane; (B) LNC membrane with LNC/Pt layer after operation under air/50%CH_4-50%He gradient at 1023–1173 K; (C) LSCG membrane with platinum layer after operation under air/50%CH_4-50%He gradient at 1123–1223 K.

controllers; the volume ratio CH_4 : He was 50 : 50 vol%. The flow rate at the outlet, measured by a soap-film flowmeter, varied in the range of 2–7 cm^3/min. The gas mixtures at the inlet and outlet were analyzed using a Varian CP-3800 gas chromatograph, equipped with thermal-conductivity and flame-ionization detectors coupled in series and a 250 μL six-port VICI gas-sampling valve. The separation and quantification of the gas components was accomplished with a semicapillary CarboPLOT P7 column using the absolute calibration method. No impurities in the initial gas mixture and also no leaking of air into the reactor were detected.

3. Results and discussion

Figures 2(B) and (C) presents SEM micrographs of LNC and LSCG membranes after the operation under air/50%CH_4-50%He gradient at 1123–1223 K during 60–100 h. No traces of bulk reduction at the membrane permeate side were found. Nonetheless, the oxygen chemical potential in the gas mixture supplied onto LNC membrane, calculated from the emf of the oxygen sensor, was slightly lower with respect to the stability limit of $La_2Ni_{0.9}Co_{0.1}O_4$ phase at 1173 K (figure 3). In the case of LSCG, the corresponding $p(O_2)$ values were 10^2–10^3 times lower than the equilibrium stability boundary in all studied temperature range.

The possibility of stable operation of the ceramic membranes, made of materials thermodynamically unstable at the permeate-side oxygen partial pressures (p_1) under equilibrium conditions, can be explained by the surface-limited oxygen transport when a membrane is placed under an oxygen chemical potential gradient. A simple model describing this behavior can be based on the transport equations analyzed in reference [25]. Figure 4 shows schematically the drop of the oxygen partial pressure across a mixed-conducting membrane.

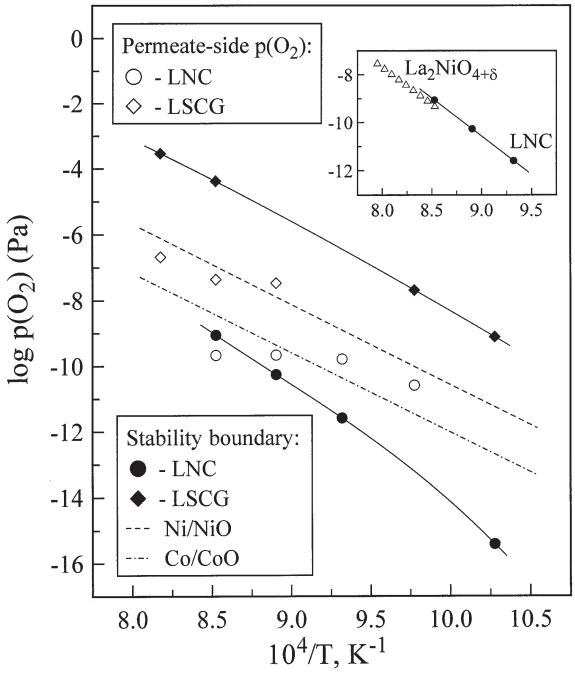

Figure 3. Stability boundaries (closed symbols) of LNC and LSCG phases, compared to the $p(O_2)$ values observed in the effluent of membrane reactors (open symbols). Inset compares LNC stability limit, determined from total conductivity (figure 1), with data on $La_2NiO_{4+\delta}$ [30]. Data on Ni/NiO and Co/CoO boundaries are taken from reference [31].

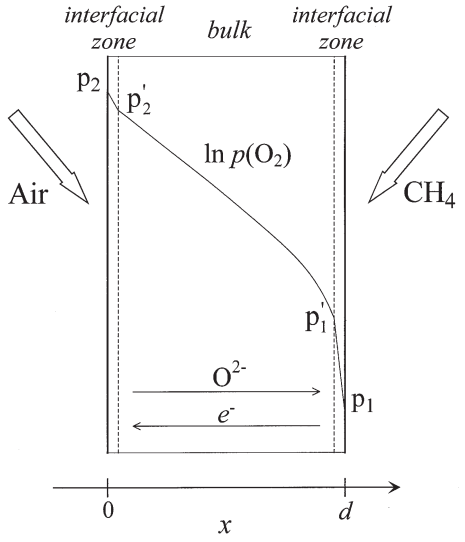

Figure 4. Oxygen chemical potential distribution in a mixed-conducting membrane with surface-limited oxygen transport.

The total $p(O_2)$ drop consists of three contributions provided by the interfacial zone at the feed side (p_2–p'_2), membrane bulk (p'_2–p'_1), and the permeate-side interfacial zone (p'_1–p_1). In the bulk, the steady state oxygen permeation flux density (j) is expressed by the integral form of Wagner equation:

$$j = \frac{RT}{16F^2 d}\int_{p'_1}^{p'_2} \sigma_{amb} d\ln p \qquad (1)$$

where d is the membrane thickness, F is the Faraday constant, R is the ideal gas constant, T is the absolute temperature, and σ_{amb} is the ambipolar conductivity, function of the partial oxygen ionic (σ_O) and electronic (σ_e) conductivities:

$$\sigma_{amb} = \frac{\sigma_O \sigma_c}{\sigma_O + \sigma_e} \qquad (2)$$

The oxygen flux through gas/membrane interface is determined by the oxygen chemical potential difference and can be nominally expressed using a similar equation [25]. For example, for the permeate side

$$j = \frac{RT}{16F^2} k_{ex} \ln\frac{p'_1}{p_1} \qquad (3)$$

where k_{ex} is constant, equal to reciprocal surface area-specific resistance to the permeation flux expressed in electrical units.

The oxygen chemical potential drop between the permeate-side membrane surface and the gas phase, calculated using equations (1–3) and expressed as $\log(p'_1/p_1)$, is shown in figure 5 as a function of the ratio between interfacial and membrane bulk resistances to oxygen transport at fixed p'_2. As expected, the difference of p'_1 and p_1 values increases with increasing total $p(O_2)$ gradient and with increasing $\int_0^d \sigma_{amb}\,dx/(d \times k_{ex})$ ratio.

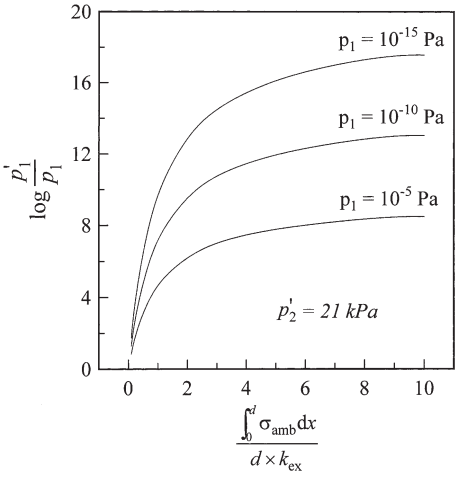

Figure 5. Calculated oxygen chemical potential drop in the permeate-side interfacial zone as a function of the ratio between interfacial and bulk resistances to oxygen transport (see text and figure 4).

The latter quantity reflects the relative role of the surface exchange limitations to oxygen transport. Therefore, when the permeation is controlled by kinetics of surface processes, either recombination of lattice oxygen into gaseous O_2 or oxidation reactions on the membrane surface, the oxygen chemical potential on the membrane permeate side should be higher than that in the gas environment. This should lead to kinetic stabilization of the membrane under nonequilibrium conditions, preventing reduction of the mixed-conducting material.

In this case, decreasing membrane thickness might be very favorable. As an example, figure 6 presents the calculated dependence of oxygen partial pressure drop at the permeate-side interfacial zone for a hypothetical mixed conductor, properties of which are given in the legend. The oxygen ionic conductivity is assumed to be $p(O_2)$-independent; the electronic transport is p-type and is expressed by a classic power model, in agreement with experimental data (figure 1). Although these estimations are rough, the results clearly indicate that

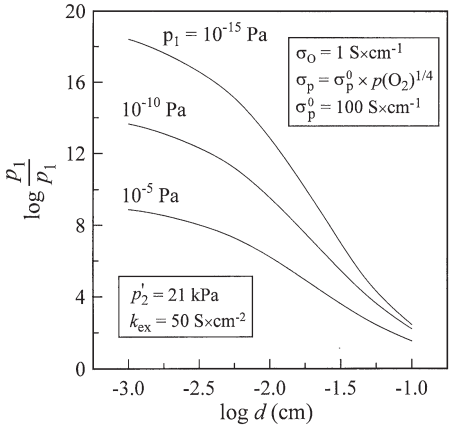

Figure 6. Calculated oxygen chemical potential drop in the permeate-side interfacial zone as a function of membrane thickness for one hypothetical material at constant feed-side oxygen pressure.

the $p(O_2)$ drop in the interfacial zone should increase with decreasing membrane thickness. This should provide higher kinetic stability for thinner membranes, which also show higher permeation fluxes as follows from equations (1) and (3).

The oxygen permeation through $SrCoO_3$- and La_2NiO_4-based mixed conductors is known to be strongly affected by the surface exchange kinetics (e.g. [20,21,24] and references cited); as a rule, the limiting role of surface processes increases with decreasing temperature and reducing oxygen partial pressure. In particular, the permeation fluxes through LNC ceramics under air/(H_2-H_2O) gradient at 973 K are determined by the hydrogen oxidation rate on the surface [21]. Hence, stable operation of LNC and LSCG membranes under air/CH_4 gradient at 1123–1223 K is achieved because of surface limitations, namely, kinetics of the oxidation reactions on the membrane permeate-side surface.

Selected results on dry methane oxidation in the membrane reactors are shown in figures 7 and 8. Owing to increasing oxygen permeation fluxes, the methane conversion efficiency increases with temperature. Under similar conditions, the conversion on LSCG membranes is approximately two times higher compared to that observed for LNC. This is obviously associated with the higher oxygen permeability of the former, as illustrated by the inset in figure 7. The selectivity with respect to carbon monoxide is, however, low for both mixed conductors. At 1173 K, the yield of CO achieved with LNC and LSCG membranes is 17% and 2% respectively. In the studied temperature range, the selectivity to C_2 hydrocarbons was less than 1–3% and decreased with temperature.

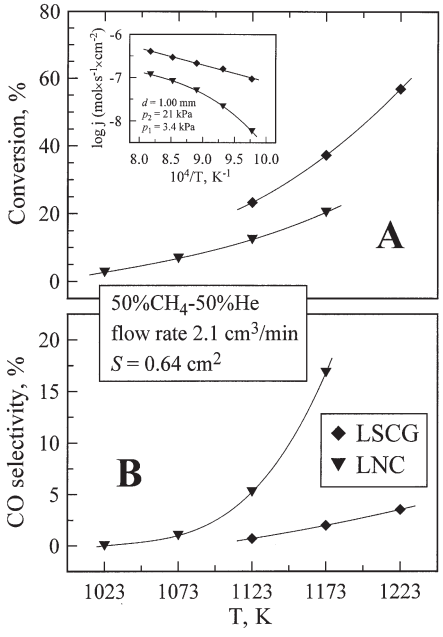

Figure 7. Temperature dependence of methane conversion (A) and CO selectivity (B) for LNC and LSCG membranes. Inset shows temperature dependence of oxygen permeation fluxes through LNC and LSCG ceramics under fixed $p(O_2)$ gradient.

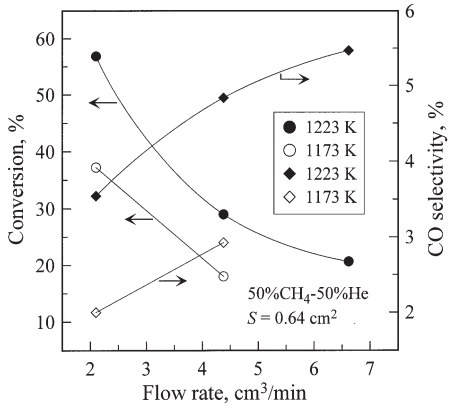

Figure 8. Dependence of CH_4 conversion and CO selectivity on the reactant flow supplied onto LSCG membrane.

One should mention that the composition of product mixtures is far from thermodynamic equilibrium, calculated neglecting formation of carbon and C_2 products. For the conversion efficiency values observed experimentally, equilibrium CO selectivity should be close to 100%. Also, a considerably higher conversion should be expected for the observed values of oxygen chemical potential in the effluent gas mixture (figure 3). This behavior seems to be in agreement with the CCR (combustion and reforming reaction) mechanism of the catalytic partial oxidation of methane [26]. The CCR mechanism involves full oxidation of methane to carbon dioxide and steam, followed by subsequent reforming of residual CH_4 with CO_2 and H_2O into CO and H_2. In the case of disk-shaped membrane reactor used in this work, the volume of porous catalyst on the membrane surface is substantially lower than the total cell volume; a significant part of methane may pass through the reactor not participating in reactions on the catalyst surface. Since no traces of O_2 were detected in the effluent stream, all permeated oxygen was probably consumed at the first stage of reaction, full combustion; the second stage, reforming, then occurs in the gas phase. This may result in nonequilibrium composition of the product mixtures, particularly in the low conversion and CO selectivity as compared to thermodynamic equilibrium values. Such a conclusion agrees with the variations of conversion and selectivity versus ratio between the inlet CH_4 and oxygen fluxes. Increasing CH_4 flow rate decreases conversion, but increases CO yield (figure 8); in fact, the product concentrations become closer to thermodynamic equilibrium. Analogously, the higher oxygen permeability of LSCG with respect to LNC membranes leads to a lower CH_4/O_2 ratio and higher methane conversion, but causes lower CO selectivity in the former case (figure 7).

A very similar behavior was observed for the YSZ reactor with cermet CGO/Pt anode (figure 9). At fixed CH_4 flow rate, the methane conversion increases with increasing oxygen flux electrochemically pumped through solid electrolyte, while the CO selectivity

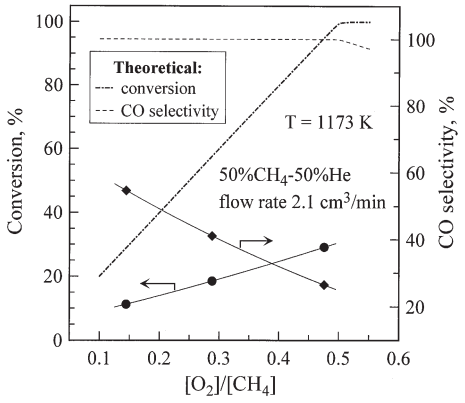

Figure 9. Dependence of CO selectivity and CH_4 conversion on the $[O_2]/[CH_4]$ molar ratio in a SOFC-type reactor with CGO/Pt anode. Thermodynamic equilibrium values are shown as dashed lines.

decreases. The overall reaction is shifted toward complete oxidation; the conversion and CO yield both are much lower than theoretical equilibrium values. Notice that these data are in excellent agreement with literature. For instance, adding of 2 wt% ceria into the platinum anode of a SOFC-type reactor was reported to decrease conversion efficiency from 75 to 28% and CO yield from 69 to ~1% [5]. At the same time, direct conversion of methane into H_2 and CO was demonstrated on $CeO_{2-\delta}$ in the absence of gaseous oxygen [27]; Pt/CeO_2 catalysts exhibit a high catalytic activity for the partial oxidation in packed-bed reactors with CH_4 and O_2 co-fed into the reaction zone [28,29]. Most probably, the low selectivity toward CO formation on ceria-containing anodes results from changes in the reaction mechanism when oxygen is electrochemically supplied through the solid electrolyte.

In summary, surface-limited oxygen permeation makes it possible to achieve kinetic stability of mixed-conducting membranes placed under an oxygen chemical potential gradient. This enables to use membrane materials with high oxygen permeability, such as $La_{0.3}Sr_{0.7}Co_{0.8}Ga_{0.2}O_{3-\delta}$ and $La_2Ni_{0.9}Co_{0.1}O_{4+\delta}$, which are thermodynamically unstable in highly reducing atmospheres under equilibrium conditions. On the other hand, the reactors with either mixed-conducting or solid-electrolyte membranes show high CO_2 yields, probably due to complete methane oxidation dominating on the membrane surface. Such behavior leads to the necessity to incorporate selective reforming catalysts into reactors. One promising approach may refer to the fabrication of dense thin membranes on highly porous ceramics, simultaneously acting as catalyst support.

Acknowledgments

This research was partially supported by the FCT, Portugal (projects POCTI/CTM/3938/2001, BPD/11606/2002 and BD/6827/2001), the NATO Science for Peace program (project 978002), and the INTAS (project 00276).

References

[1] D.J. Wilhelm, D.R. Simbeck, A.D. Karp and R.L. Dickenson, Fuel Process. Technol. 71 (2001) 139.
[2] J.R. Rostrup-Nielsen, Catal. Today 71 (2002) 243.
[3] P.N. Dyer, R.E. Richards, S.L. Russek and D.M. Taylor, Solid State Ionics 134 (2000) 21.
[4] V. Antonucci, P.L. Antonucci, A.S. Aricò and N. Giordano, J. Power Sources 63 (1996) 95.
[5] V.A. Sobyanin, V.D. Belyaev and V.V. Gal'vita, Catal. Today 42 (1998) 337.
[6] S. Pei, M.S. Kleefisch, T.P. Kobylinski, J. Faber, C.A. Udovich, V. Zhang-McCoy, B. Dabrowski, U. Balachandran, R.V. Mieville and R.B. Poeppel, Catal. Lett. 30 (1995) 201.
[7] J.E. ten Elshof, B.A. van Hassel and H.J.M. Bouwmeester, Catal. Today 25 (1995) 397.
[8] C.Y. Tsai, A.G. Dixon, Y.H. Ma, W.R. Moser and M.R. Pascucci, J. Am. Ceram. Soc. 81 (1998) 1437.
[9] W. Jin, S. Li, P. Huang, N. Xu, J. Shi and Y.S. Lin, J. Membr. Sci. 166 (2000) 13.
[10] S.J. Xu and W.J. Thomson, AlChE J. 43 (1997) 2731.
[11] Y. Zeng, Y.S. Lin and S.L. Swartz, J. Membr. Sci. 150 (1998) 87.
[12] O. Yamamoto, Electrochim. Acta 45 (2000) 2423.
[13] R.M. Ormerod, Chem. Soc. Rev. 32 (2003) 17.
[14] R.J. Gorte, H. Kim and J.M. Vohs, J. Power Sources 106 (2002) 10.
[15] T. Tsai and S.A. Barnett, Solid State Ionics 98 (1997) 191.
[16] V.V. Kharton, E.N. Naumovich, V.N. Tikhonovich, I.A. Bashmakov, L.S. Boginsky and A.V. Kovalevsky, J. Power Sources 79 (1999) 242.
[17] X.G. Wang, N. Nakagawa and K. Kato, Electrochemistry 70 (2002) 252.
[18] E. Ramirez-Cabrera, A. Atkinson and D. Chadwick, Solid State Ionics 136–137 (2000) 825.
[19] T. Nakamura, G. Petzov and L.J. Gaukler, Mater. Res. Bull. 15 (1979) 649.
[20] V.V. Kharton, A.V. Kovalevsky, A.A. Yaremchenko, F.M. Figueiredo, E.N. Naumovich, A.L. Shaulo and F.M.B. Marques, J. Membr. Sci. 195 (2002) 277.
[21] A.A. Yaremchenko, V.V. Kharton, M.V. Patrakeev and J.R. Frade, J. Mater. Chem. 13 (2003) 1136.
[22] V.V. Kharton, A.A. Yaremchenko, M.V. Patrakeev, E.N. Naumovich and F.M.B. Marques, J. Eur. Ceram. Soc. 23 (2003) 1417.
[23] L.A. Chick, L.R. Pederson, G.D. Maupin, J.L. Bates, L.E. Thomas and G.L. Exarhos, Mater. Lett. 10 (1990) 6.
[24] V.V. Kharton, V.N. Tikhonovich, L. Shuangbao, E.N. Naumovich, A.V. Kovalevsky, A.P. Viskup, I.A. Bashmakov and A.A. Yaremchenko, J. Electrochem. Soc. 145 (1998) 1363.
[25] H.J.M. Bouwmeester, H. Kruidhof and A.J. Burggraaf, Solid State Ionics 72 (1994) 185.
[26] A.G. Steghuis, J.G. van Ommen, K. Seshan and J.A. Lercher, Stud. Surf. Sci. Catal. 107 (1997) 403.
[27] K. Otsuka, Y. Wang, E. Sunada and I. Yamanaka, J. Catal. 175 (1998) 152.
[28] P. Pantu and G.R. Gavalas, Appl. Catal. A 223 (2002) 253.
[29] L. Pino, A. Vita, M. Cordaro, V. Recupero and M.S. Hegde, Appl. Catal. A 243 (2003) 135.
[30] D.E. Rice and D.J. Buttrey, J Solid State Chem. 105 (1993) 197.
[31] H.S. O'Neill and M.I. Pownceby, Contrib. Mineral. Petrol. 114 (1993) 296.